

Behaviour of the Serre Equations in the Presence of Steep Gradients Revisited

J.P.A. Pitt^{a,*}, C. Zoppou^a, S.G. Roberts^a

^a*Mathematical Sciences Institute, Australian National University, Canberra, ACT 0200, Australia*

Abstract

We use numerical methods to study the behaviour of the Serre equations in the presence of steep gradients because there are no known analytical solutions for these problems. In keeping with the literature we study a class of initial condition problems that are a smooth approximation to the initial conditions of the dam-break problem. This class of initial condition problems allow us to observe the behaviour of the Serre equations with varying steepness of the initial conditions. The numerical solutions of the Serre equations are justified by demonstrating that as the resolution increases they converge to a solution with little error in conservation of mass, momentum and energy independent of the numerical method. We observe four different structures of the converged numerical solutions depending on the steepness of the initial conditions. Two of these structures were observed in the literature, with the other two not being commonly found in the literature. The numerical solutions are then used to assess how well the analytical solution of the shallow water wave equations captures the mean behaviour of the solution of the Serre equations for the dam-break problem. Lastly the numerical solutions are used to evaluate the usefulness of asymptotic results in the literature to approximate the depth and location of the front of an undular bore.

Keywords: Serre equations, steep gradients, dam break

¹ 1. Introduction

² The behaviour of flows containing steep gradients are important to a range of problems in shallow water such as the propagation of a bore, the dam-break problem and
³ shoaling waves on a beach.

⁵ The Serre equations are used as a compromise between the non-dispersive shallow
⁶ water wave equations and the incompressible inviscid Euler equations for modelling
⁷ dispersive waves of the free surface in the presence of steep gradients, which are
⁸ present for the Euler equations [1] but not for the shallow water wave equations. The

*Corresponding author

Email addresses: jordan.pitt@anu.edu.au (J.P.A. Pitt),
christopher.zoppou@anu.edu.au (C. Zoppou), stephen.roberts@anu.edu.au
(S.G. Roberts)

9 Serre equations like the shallow water wave equations produce methods [2–4] that are
10 computationally easier and quicker to solve than the best methods for the Euler equa-
11 tions. The Serre equations are considered the most appropriate approximation to the
12 Euler equations for modelling dispersive waves up to the shore line [5, 6]. Therefore,
13 understanding the behaviour of the Serre equations in the presence of steep gradients
14 offers some insight into the behaviour of steep gradients for fluids more generally.

15 There are no known analytical solutions to problems containing steep gradients for
16 the Serre equations. To infer the structure of solutions to problems containing steep
17 gradients we have to resort to investigating numerical solutions of the Serre equations
18 for these problems.

19 There are few examples in the literature which depict the behaviour of numerical
20 solutions to the Serre equations in the presence of steep gradients [1–4, 7, 8]. These
21 papers all present problems with discontinuous initial conditions [2–4] or a smooth
22 approximation to them when the numerical method requires some smoothness of the
23 solutions [1, 7, 8]. Among these papers there are differences in the structures of the nu-
24 matical solutions, with some demonstrating undulations in depth and velocity through-
25 out the bore [3, 4, 7] and others showing a constant depth and velocity state in the
26 middle of the bore [1, 2, 8].

27 The mean behaviour of numerical solutions to the dam-break problem for the Serre
28 equations is consistent across the literature [1–4, 7, 8] and was demonstrated to be
29 well approximated by the analytical solution to the dam-break problem by the shallow
30 water wave equations [2, 8]. Expressions for the leading wave amplitude and speed of
31 an undular bore for the Serre equations were derived and verified for a range of undular
32 bores by El et al. [7]. These expressions were also shown to be valid for all the different
33 structures found in the literature [7, 8].

34 The first aim of this paper is to investigate and explain why different behaviour
35 has been published in the literature for numerical solutions of the Serre equations for
36 problems containing steep gradients. We find that the undulations of a bore can be
37 damped to a constant depth and velocity state by the numerical diffusion introduced by
38 the method, as is the case for Le Métayer et al. [2]. Oscillation damping can also occur
39 due to the particular smoothing of the initial conditions, as is the case for Mitsotakis
40 et al. [1], El et al. [7] and Mitsotakis et al. [8]. We do find that over long time periods
41 the Serre equations damp these oscillations as they propagate, but this natural decay is
42 dominated by other factors in the literature.

43 The second aim of this paper is to assess the utility of the shallow water wave
44 equations and the results of El et al. [7] as guides for the evolution of an undular bore.
45 We find that for a range of dam-break problems the analytical solution of the shallow
46 water wave equations is a good approximation for the mean depth and velocity of the
47 Serre equations, extending the findings of Le Métayer et al. [2] and Mitsotakis et al. [8]
48 to a larger range of dam-break problems. It was also found that the results of El et al.
49 [7] are a good approximation to our numerical solutions.

50 The first aim of this paper is achieved by demonstrating that our numerical solutions
51 are good approximations to the true solutions of the Serre equations. This is accom-
52 plished by demonstrating that as the resolution of a particular method is increased, the
53 numerical solutions converge to a numerical solution with little error in the conserva-
54 tion of mass, momentum and energy. The numerical solution is also consistent across

55 the five different numerical methods. Three of the methods are the first, second and
 56 third-order methods presented by Zoppou et al. [4]. The first-order method is equivalent
 57 to the method of Le Métayer et al. [2]. The fourth method is a recreation of the
 58 second-order method used by El et al. [7]. Lastly, the fifth method is a second-order
 59 finite difference approximation to the Serre equations.

60 The second aim is accomplished by comparing our verified numerical solutions to
 61 the analytical solutions of the shallow water wave equations and the Whitham modula-
 62 tion results presented by El et al. [7].

63 The paper is organised as follows, in Section 2 the Serre equations and the quan-
 64 tities they conserve are presented. In Section 3 the smoothed dam-break problem is
 65 defined, the measures of the relative difference between numerical solutions and the
 66 relative error in the conserved quantities are presented. The analytical solution of the
 67 shallow water wave equations and the expressions for the amplitude and speed of the
 68 leading wave of an undular bore are presented. In Section 4 the numerical methods and
 69 their important properties are presented. In Section 5 the four different structures in
 70 the solutions of smoothed dam-break problem for the Serre equations are determined
 71 using verified numerical solutions. The verified numerical solutions are also used to
 72 evaluate how well the analytical solution of the shallow water wave equations captures
 73 the mean behaviour of the solution of the Serre equations for the dam-break problem.
 74 The Whitham modulations results are also compared to the verified numerical solutions
 75 to test their veracity.

76 2. Serre Equations

77 The Serre equations can be derived by integrating the full inviscid incompressible
 78 Euler equations over the water depth [9]. They can also be derived as an asymptotic
 79 expansion of the Euler equations [10]. Assuming a constant horizontal bed, the one-
 80 dimensional Serre equations are [11]

$$81 \quad \frac{\partial h}{\partial t} + \frac{\partial(uh)}{\partial x} = 0 \quad (1a)$$

83 and

$$84 \quad \underbrace{\frac{\partial(uh)}{\partial t} + \frac{\partial}{\partial x} \left(u^2 h + \frac{gh^2}{2} \right)}_{\text{Shallow Water Wave Equations}} + \underbrace{\frac{\partial}{\partial x} \left(\frac{h^3}{3} \left[\frac{\partial u}{\partial x} \frac{\partial u}{\partial x} - u \frac{\partial^2 u}{\partial x^2} - \frac{\partial^2 u}{\partial x \partial t} \right] \right)}_{\text{Dispersion Terms}} = 0. \quad (1b)$$

85 $\overbrace{\hspace{30em}}$ Serre Equations

86 Where $u(x, t)$ is the horizontal velocity over the depth of water $h(x, t)$, g is the acceler-
 87 ation due to gravity, x is the horizontal spatial variable and t is time.

88 The Serre equations are conservation laws for ‘mass’ (1a), ‘momentum’ (1b) and
 89 the Hamiltonian [12, 13]

$$90 \quad \mathcal{H}(x, t) = \frac{1}{2} \left(hu^2 + \frac{h^3}{3} \left(\frac{\partial u}{\partial x} \right)^2 + gh^2 \right) \quad (2)$$

92 which is the total energy.

93 The total amount of a quantity q in a system in the spatial interval $[a, b]$ at a partic-
94 ular time t , is measured by

95
$$C_q(t) = \int_a^b q(x, t) dx.$$

96

97 Conservation of a quantity q implies that $C_q(0) = C_q(t)$ for all t provided the interval is
98 fixed and the system is closed. Our numerical methods should demonstrate conserva-
99 tion for the quantities h , uh and \mathcal{H} .

100 **3. Smoothed Dam Break Problem**

101 In this section we define a class of initial condition problems, called the smoothed
102 dam-break problem that we use throughout our numerical investigation. This class of
103 initial conditions are used in the literature [1, 8] to smoothly approximate the discontinu-
104 ous initial conditions of the dam-break problem, as some numerical methods require
105 smoothness of the solutions.

106 The smoothed dam-break problem has the following initial conditions

107
$$h(x, 0) = h_0 + \frac{h_1 - h_0}{2} \left(1 + \tanh\left(\frac{x_0 - x}{\alpha}\right) \right) m, \quad (3a)$$

108

109 and

110
$$u(x, 0) = 0.0 \text{ m/s}. \quad (3b)$$

111

112 This represents a smooth transition centred around x_0 between a water depth of h_0
113 on the right which is smaller than the water depth of h_1 on the left. Here α measures
114 the distance over which approximately 46% of that smooth transition between the two
115 heights occurs. Decreasing α increases the steepness of the initial conditions as can be
116 seen in Figure 1 where $h_0 = 1m$ and $h_1 = 1.8m$. These are the same h_0 and h_1 values as
117 those of the smoothed dam-break problem of El et al. [7] and the dam-break problem
118 of Le Métayer et al. [2].

119 There are no known analytical solutions of the Serre equations for the dam-break
120 problem or an arbitrary smoothed dam-break problem. Therefore, to demonstrate that
121 our numerical solutions converge we use the relative difference between numerical
122 solutions. To demonstrate that our numerical solutions also have small errors in the
123 conserved quantities we use the relative error of their conservation. Both of these
124 measures are defined in this section.

125 *3.1. Assessing validity of Numerical Solutions*

126 To demonstrate that our numerical solutions converge to a solution with little error
127 in the conserved quantities as the spatial resolution is increased we use two measures;
128 the relative difference between numerical solutions of different resolutions and the error
129 in the conservation of a quantity. The relative difference between numerical solutions

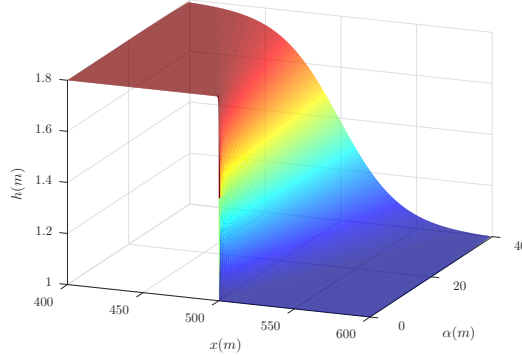


Figure 1: Initial conditions for smooth dam-break problems with $h_0 = 1m$, $h_1 = 1.8m$, $x_0 = 500m$ and various α .

measures their convergence, while the error in conservation measures how well the numerical solutions conserve the quantities h , uh and \mathcal{H} .

We introduce the following notation for the spatial grids defined by x_i and the temporal grids defined by t^n upon which the numerical solutions are calculated. These grids are uniform so that $\Delta x = x_i - x_{i-1}$ for all i and $\Delta t = t^n - t^{n-1}$ for all n . We use subscripts and superscripts to denote where a quantity q is evaluated in the following way $q_i^n = q(x_i, t^n)$. Finally, the i th cell is the interval $[x_i - \Delta x/2, x_i + \Delta x/2]$ centred around x_i .

3.1.1. Convergence of Numerical Results

To measure the convergence of the numerical solutions we ensured all grids had common locations to compare them by dividing Δx by 2 to create finer grids. Therefore, the finest grid with the smallest Δx contains all the locations x_i in any coarser grid. To measure the relative difference between quantities on these grids we compare them only on the coarser grid points x_i . For some quantity q we have our numerical approximation to it on the finest grid q^* and on the coarser grid q' , with the relative difference between the two being

$$L_1^q = \frac{\sum_i |q'(x_i) - q^*(x_i)|}{\sum_i |q^*(x_i)|}. \quad (4)$$

3.1.2. Conserved Quantities

To calculate the error in conservation of a quantity, we must first calculate the total amount of the conserved quantities for the initial conditions. For the smoothed dam-break problem the initial conditions (3) were integrated to obtain expressions for the total mass $C_h(0)$, the total momentum $C_{uh}(0)$ and the total Hamiltonian $C_{\mathcal{H}}(0)$. Provided x_0 is the midpoint of the spatial domain $[a, b]$ the total amounts for the conserved quantities are

$$C_h(0) = \frac{h_1 + h_0}{2} (b - a),$$

157

158

$$C_{uh}(0) = 0$$

160 and

$$161 \quad C_{\mathcal{H}}(0) = \frac{g}{4} \left(h_0^2 - h_1^2 + \alpha (h_1 - h_0)^2 \tanh \left(\frac{a-b}{2\alpha} \right) \right). \\ 162$$

163

164 To calculate how well we approximate the total amount of a quantity q in our
 165 numerical solution we fit a quartic interpolant of the primitive variables h and u over a
 166 cell utilising neighbouring cells and then apply Gaussian quadrature with 3 points. The
 167 amount of q in each cell is summed across all cells to get the total amount of q in
 168 our numerical solution at time t , which we call $C_q^*(t)$. The error in conservation of a
 169 quantity q for a numerical solution is

$$170 \quad C_1^q = \frac{|C_q(0) - C_q^*(t)|}{|C_q(0)|}. \\ 171 \quad (6)$$

172 Note that for uh the denominator is 0 and that there is a flux of momentum due to the
 173 unequal heights at both ends of the domain. To resolve this issue for uh the error in the
 174 conservation of uh is measured by

$$175 \quad C_1^{uh} = \left| C_{uh}(0) - C_{uh}^*(t) - \frac{gt}{2} (h(b)^2 - h(a)^2) \right|. \\ 176 \quad (7)$$

177 3.2. Background for derived and observed comparisons

178 It was demonstrated by Le Métayer et al. [2] and Mitsotakis et al. [8] that the
 179 analytical solution of the shallow water wave equations for the dam-break problem
 180 captures the mean behaviour of the numerical solutions of the Serre equations to the
 181 dam-break problem [2] and the smoothed dam-break problem [8].

182 El et al. [7] derived an expression for the long term amplitude of the leading wave
 183 of an undular bore A^+ for the Serre equations. Since the front of an undular bore
 184 decomposes into solitons, the speed of the leading wave S^+ can be calculated from its
 185 amplitude.

186 To be self contained we present the analytical solution of the shallow water wave
 187 equations to the dam-break problem and the expressions derived by El et al. [7].

188 3.2.1. Shallow Water Wave Equation Analytical Solution

189 For the dam-break problem the shallow water wave equations, which are the Serre
 190 equations with dispersive terms neglected, can be solved analytically.

191 An example of the analytical solution of the shallow water wave equations for the
 192 dam-break problem is presented in Figure 2. Region I is the undisturbed water up-
 193 stream of the dam-break at constant height (h_1) and velocity (0m/s). Region II is the
 194 rarefaction fan connecting regions I and III. Regions III and IV represent the shock
 195 with constant height (h_2) and constant velocity (u_2), these regions are separated by
 196 $x_{u_2} = x_0 + u_2 t$. Region V is the undisturbed water downstream at constant height (h_0)

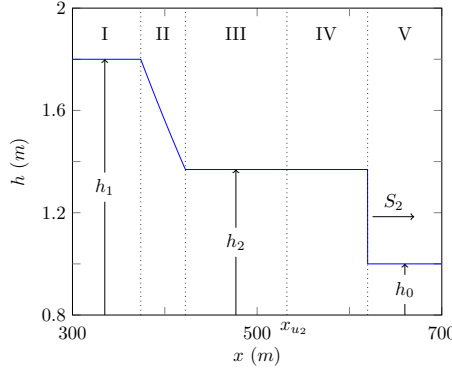


Figure 2: Analytical solution at $t = 30s$ of the dam-break problem for the shallow water wave equations with $h_0 = 1m$, $h_1 = 1.8m$ and $x_0 = 500m$.

and velocity ($0m/s$) separated from Region IV by a shock which travels at velocity S_2 . Expressions for the unknown quantities h_2 , u_2 and S_2 in terms of h_0 and h_1 were given by Wu et al. [14] as

$$h_2 = \frac{h_0}{2} \left(\sqrt{1 + 8 \left(\frac{2h_2}{h_2 - h_0} \frac{\sqrt{h_1} - \sqrt{h_2}}{\sqrt{h_0}} \right)^2} - 1 \right), \quad (8a)$$

$$u_2 = 2 \left(\sqrt{gh_1} - \sqrt{gh_2} \right) \quad (8b)$$

and

$$S_2 = \frac{h_2 u_2}{h_2 - h_0}. \quad (8c)$$

Applying (8) to our dam-break heights of interest; $h_0 = 1m$ and $h_1 = 1.8m$ results in $h_2 = 1.36898m$, $u_2 = 1.074975 m/s$ and $S_2 = 3.98835 m/s$ which are shown in Figure 2 for $t = 30s$. The location of the front of the bore for the shallow water wave equations at time t is thus $x_{S_2}(t) = x_0 + S_2 t$ so that $x_{S_2}(30s) = 619.6505m$.

3.2.2. Whitham Modulation for Undular Bores of the Serre Equations

Utilizing Whitham modulation theory for a one-phase periodic travelling wave an asymptotic analytical expression for the amplitude A^+ and speed S^+ of the leading wave was derived by El et al. [7]. An example of an undular bore is shown in Figure 3. The derived expressions for A^+ and S^+ are

$$\frac{\Delta}{(A^+ + 1)^{1/4}} - \left(\frac{3}{4 - \sqrt{A^+ + 1}} \right)^{21/10} \left(\frac{2}{1 + \sqrt{A^+ + 1}} \right)^{2/5} = 0 \quad (9a)$$

and

$$S^+ = \sqrt{g(A^+ + 1)} \quad (9b)$$

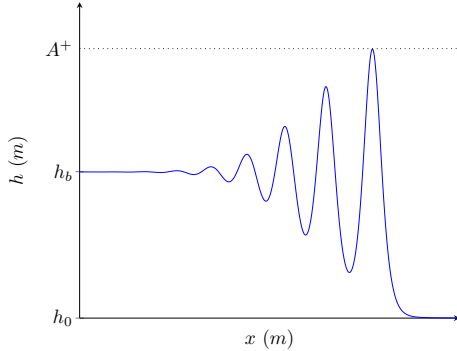


Figure 3: Demonstration of quantities obtained by Whitham modulation for undular bores of the Serre equations.

where $\Delta = h_b/h_0$, and h_b is the height of the bore. The height of the bore created by the dam-break problem in (9a) used by El et al. [7] was

$$h_b = \frac{1}{4} \left(\sqrt{\frac{h_1}{h_0}} + 1 \right)^2.$$

For our dam-break heights of interest $h_0 = 1m$ and $h_1 = 1.8m$ we obtain $h_b = 1.37082m$, $\Delta = 1.37082$, $A^+ = 1.73998m$ and $S^+ = 4.13148m/s$. The location of the leading wave of an undular bore at time t is then $x_{S^+}(t) = x_0 + S^+t$ so that $x_{S^+}(30s) = 623.9444m$.

4. Numerical Methods

Five numerical schemes were used to investigate the behaviour of the Serre equations in the presence of steep gradients, the first (\mathcal{V}_1), second (\mathcal{V}_2) and third-order (\mathcal{V}_3) finite difference finite volume methods of Zoppou et al. [4], the second-order finite difference method of El et al. [7] (\mathcal{E}) and a second-order finite difference method (\mathcal{D}) that can be found in the Appendix.

The \mathcal{V}_i methods are stable under a Courant-Friederichs-Lowy (CFL) condition presented by A. Harten [15]. The \mathcal{V}_i methods have demonstrated the appropriate order of convergence for smooth problems [4]. Furthermore, \mathcal{V}_2 and \mathcal{V}_3 have been validated against experimental data containing steep gradients [4]. The two methods \mathcal{D} and \mathcal{E} were found to be stable under the same CFL condition.

Generally, we found that \mathcal{V}_1 is the worst performing method due to its numerical diffusion [4]. Of the high-order methods \mathcal{E} is the worst performing, introducing dispersive errors.

5. Numerical Results

We investigate the behaviour of the Serre equations in the presence of steep gradients by numerically solving the smoothed dam-break problem while varying the steepness of the initial conditions. As $\Delta x \rightarrow 0$ our numerical solutions should represent

244 a good approximation of the true solution of the Serre equations. If our numerical
245 solutions to a smoothed dam-break problem converge to the same numerical solution
246 with little error in conservation of mass, momentum and energy as $\Delta x \rightarrow 0$ for each
247 method, then this numerical solution is considered an accurate approximate solution to
248 that smoothed dam-break problem for the Serre equations.

249 This process validates our numerical solutions for the smoothed dam-break prob-
250 lem, and thus validates our numerical methods to approximate the solution of the Serre
251 equations in the presence of steep gradients, if it exists. With a validated model we can
252 compare the numerical solution to the analytical solution of the shallow water wave
253 equations for the dam-break problem and the results of El et al. [7].

254 Throughout most of this section we are interested in the numerical solution at $t =$
255 $30s$ to the smoothed dam-break problem with $h_0 = 1m$, $h_1 = 1.8m$ and $x_0 = 500m$
256 while allowing for different α values. All numerical methods used $\Delta t = 0.01\Delta x$ which
257 is smaller than required by the CFL condition, ensuring stability of our schemes. The
258 method \mathcal{V}_2 requires an input parameter to its slope limiter and this was chosen to be
259 $\theta = 1.2$ [4]. The spatial domain was $[0m, 1000m]$ with the following Dirichlet boundary
260 conditions, $u = 0m/s$ at both boundaries, $h = 1.8m$ on the left and $h = 1m$ on the right.

261 *5.1. Observed Structures of the Numerical Solutions*

262 We observe that there are four different structures for the converged to numerical
263 solution depending on the chosen α . They are the ‘non-oscillatory’ structure \mathcal{S}_1 , the
264 ‘flat’ structure \mathcal{S}_2 , the ‘node’ structure \mathcal{S}_3 and the ‘growth’ structure \mathcal{S}_4 . An example
265 of each of these structures is shown in Figure 4 which were obtained using \mathcal{V}_3 with
266 $\Delta x = 10/2^{11}m$.

267 The four structures are identified by the dominant features of the numerical solu-
268 tions in regions III and IV. They also correspond to different structures in the numerical
269 solutions that have been presented in the literature. From Figure 4 it can be seen that as
270 α is decreased, steepening the initial conditions, the numerical solutions demonstrate
271 an increase in the size and number of oscillations particularly around x_{u_2} . We observe
272 that the difference between \mathcal{S}_2 , \mathcal{S}_3 and \mathcal{S}_4 is the amplitude of the oscillations in regions
273 III and IV.

274 For the non-oscillatory and flat structures there is excellent agreement between all
275 higher-order numerical methods at our highest resolution $\Delta x = 10/2^{11}m$. An illustra-
276 tion of this agreement is given in Figure 5 for \mathcal{S}_2 which is the most difficult to resolve of
277 the two structures. However, the first-order method \mathcal{V}_1 suppresses oscillations present
278 in the numerical solutions of other methods due to its diffusive errors [4]. To resolve
279 these oscillations with \mathcal{V}_1 much lower of values of Δx are required.

280 *5.1.1. Non-oscillatory Structure*

281 The \mathcal{S}_1 “non-oscillatory” structure is the result of a large α , which causes the front
282 of this flow to not be steep enough to generate undulations over short time periods.
283 As the system evolves the front will steepen due to non-linearity and undulations will
284 develop.

285 The structure \mathcal{S}_1 is not present in the literature as no authors chose large enough α
286 because, such a large α poorly approximates the dam-break problem. An example of

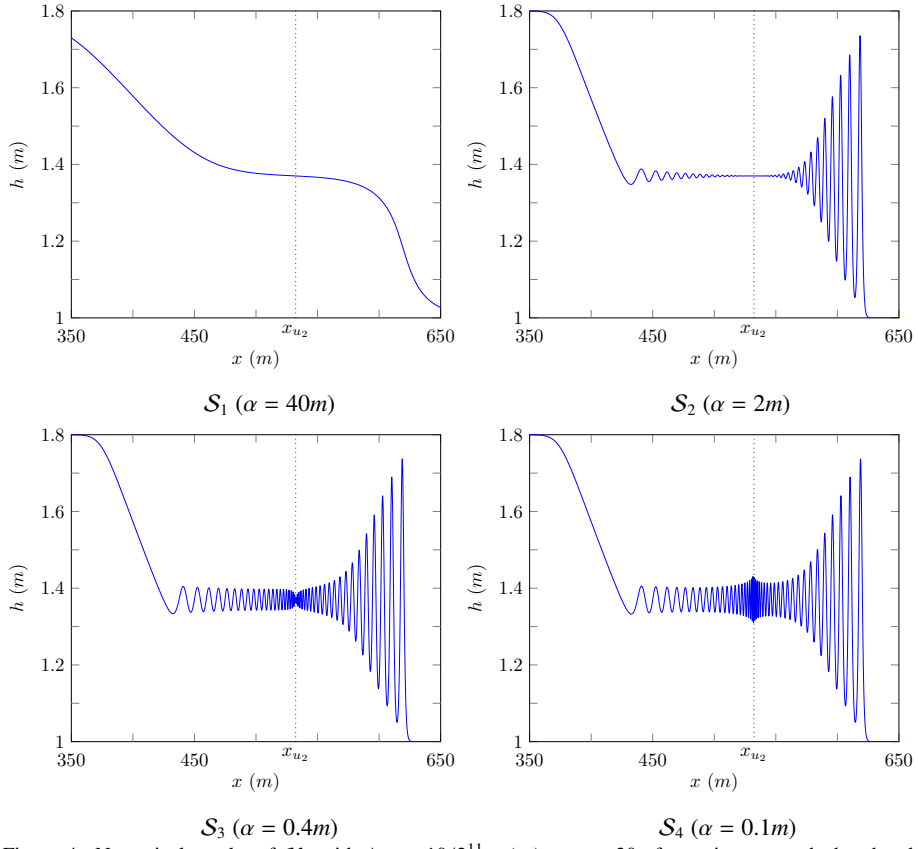


Figure 4: Numerical results of \mathcal{V}_3 with $\Delta x = 10/2^{11}m$ (blue) at $t = 30s$ for various smooth dam-break problems demonstrating the different observed structures particularly around x_{u2} (· · ·).

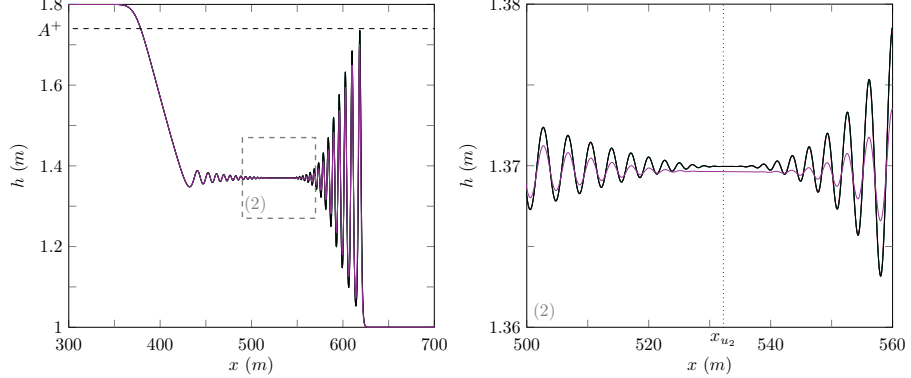


Figure 5: Numerical solutions of \mathcal{D} (blue), \mathcal{E} (red), \mathcal{V}_3 (green), \mathcal{V}_2 (black) and \mathcal{V}_1 (purple) with $\Delta x = 10/2^{11}m$ at $t = 30s$ for the smooth dam-break problem with $\alpha = 2m$. The Whitham modulation result for the leading wave height A^+ (— —) and x_{u2} (· · ·) are presented for comparison.

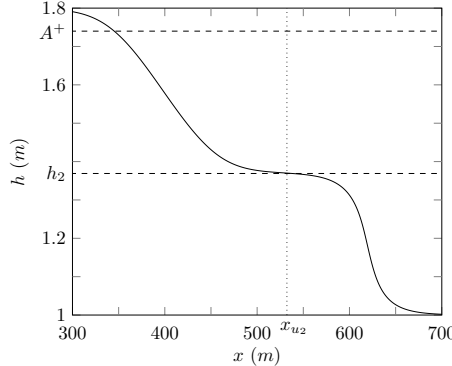


Figure 6: Numerical solutions of \mathcal{V}_3 at $t = 30s$ for smooth dam-break problem with $\alpha = 40m$ for $\Delta x = 10/2^{10}m$ (—), $10/2^8m$ (—), $10/2^6m$ (—) and $10/2^4m$ (—). The important quantities A^+ (— —), h_2 (— —) and x_{u2} (· · ·) are also presented.

287 this structure can be seen in Figure 6 for $\alpha = 40m$ using \mathcal{V}_3 with various Δx values.
 288 Because this is not a very steep problem all numerical results are visually identical for
 289 all $\Delta x < 10/2^4m$.

290 From Table 1 it can be seen that not only have these solutions converged visually but
 291 the L_1 measures demonstrate that we have reached convergence to round-off error by
 292 $\Delta x = 10/2^8m$ after which the relative difference between numerical solutions plateau.

293 Table 1 also demonstrates that the error in conservation of the numerical solutions
 294 are at round-off error for h and \mathcal{H} . The conservation of uh is poor because the smoothed
 295 dam-break has such a large α that $h(0m) \neq 1.8m$ and $h(1000m) \neq 1m$, causing unequal
 296 fluxes in momentum at the boundaries.

297 As stated above when $\Delta x = 10/2^{11}m$ the numerical solutions from all methods are
 298 identical for this smoothed dam-break problem.

299 The convergence of the numerical solutions as $\Delta x \rightarrow 0$ to a numerical solution
 300 with small error in conservation, independent of the method demonstrates that we have
 301 accurately solved the smoothed dam-break problem with $\alpha = 40m$. Therefore, the S_1
 302 structure should be observed in the solutions of the Serre equations for the smoothed
 303 dam-break problem for sufficiently large α .

304 5.1.2. Flat Structure

305 The most common structure observed in the literature [1, 2, 8] is the “flat structure”
 306 S_2 . It is observed when the initial conditions are steep enough such that the bore that
 307 develops has undulations. This structure consists of oscillations in regions III and
 308 IV which are separated by a constant height state around x_{u2} . An example of the S_2
 309 structure can be seen in the numerical solutions presented in Figure 7 where $\alpha = 2m$.

310 As Δx decreases the numerical solutions converge so that by $\Delta x = 10/2^8m$ the
 311 solutions for higher Δx are visually identical. Table 1 demonstrates that although we
 312 have convergence visually, the L_1 measures are still decreasing and are larger than
 313 round-off error. Likewise the C_1 measures are still decreasing and have only reached
 314 round-off error for h . This indicates that to attain full convergence of the numerical
 315 solutions of this smoothed dam-break problem down to round-off error using \mathcal{V}_3 would

α	Δx	C_1^h	C_1^{uh}	C_1^H	L_1^h	L_1^u
40	$10/2^4$	$2.00 \cdot 10^{-11}$	$1.77 \cdot 10^{-6}$	$1.23 \cdot 10^{-8}$	$1.74 \cdot 10^{-7}$	$2.90 \cdot 10^{-6}$
40	$10/2^6$	$1.07 \cdot 10^{-11}$	$1.50 \cdot 10^{-6}$	$1.49 \cdot 10^{-10}$	$2.57 \cdot 10^{-9}$	$4.19 \cdot 10^{-8}$
40	$10/2^8$	$8.77 \cdot 10^{-13}$	$5.49 \cdot 10^{-7}$	$3.77 \cdot 10^{-13}$	$6.08 \cdot 10^{-11}$	$5.28 \cdot 10^{-10}$
40	$10/2^{10}$	$1.77 \cdot 10^{-11}$	$2.21 \cdot 10^{-8}$	$3.56 \cdot 10^{-11}$	$2.54 \cdot 10^{-11}$	$6.49 \cdot 10^{-11}$
<hr/>						
2	$10/2^4$	$4.90 \cdot 10^{-14}$	$5.10 \cdot 10^{-3}$	$8.69 \cdot 10^{-4}$	$5.02 \cdot 10^{-3}$	$6.77 \cdot 10^{-2}$
2	$10/2^6$	$2.51 \cdot 10^{-13}$	$2.18 \cdot 10^{-4}$	$6.58 \cdot 10^{-5}$	$4.14 \cdot 10^{-4}$	$5.20 \cdot 10^{-3}$
2	$10/2^8$	$9.81 \cdot 10^{-13}$	$7.72 \cdot 10^{-7}$	$5.01 \cdot 10^{-7}$	$6.00 \cdot 10^{-6}$	$7.59 \cdot 10^{-5}$
2	$10/2^{10}$	$3.95 \cdot 10^{-12}$	$5.56 \cdot 10^{-9}$	$6.13 \cdot 10^{-9}$	$1.76 \cdot 10^{-7}$	$2.33 \cdot 10^{-6}$
<hr/>						
0.4	$10/2^4$	$9.00 \cdot 10^{-14}$	$4.82 \cdot 10^{-3}$	$1.02 \cdot 10^{-3}$	$6.79 \cdot 10^{-3} \dagger$	$9.93 \cdot 10^{-2} \dagger$
0.4	$10/2^6$	$2.40 \cdot 10^{-13}$	$2.41 \cdot 10^{-4}$	$1.11 \cdot 10^{-4}$	$8.89 \cdot 10^{-4} \dagger$	$1.13 \cdot 10^{-2} \dagger$
0.4	$10/2^8$	$9.68 \cdot 10^{-13}$	$7.57 \cdot 10^{-7}$	$2.25 \cdot 10^{-6}$	$1.53 \cdot 10^{-5} \dagger$	$1.91 \cdot 10^{-4} \dagger$
0.4	$10/2^{10}$	$3.91 \cdot 10^{-12}$	$4.95 \cdot 10^{-9}$	$2.01 \cdot 10^{-8}$	$3.61 \cdot 10^{-7} \dagger$	$5.00 \cdot 10^{-6} \dagger$
<hr/>						
0.1	$10/2^4$	$7.60 \cdot 10^{-14}$	$4.82 \cdot 10^{-3}$	$1.06 \cdot 10^{-3}$	$7.04 \cdot 10^{-3} \dagger$	$1.02 \cdot 10^{-1} \dagger$
0.1	$10/2^6$	$2.40 \cdot 10^{-13}$	$2.39 \cdot 10^{-4}$	$1.44 \cdot 10^{-4}$	$1.02 \cdot 10^{-3} \dagger$	$1.28 \cdot 10^{-2} \dagger$
0.1	$10/2^8$	$9.79 \cdot 10^{-13}$	$2.21 \cdot 10^{-7}$	$1.20 \cdot 10^{-5}$	$2.86 \cdot 10^{-5} \dagger$	$3.46 \cdot 10^{-4} \dagger$
0.1	$10/2^{10}$	$3.92 \cdot 10^{-12}$	$4.46 \cdot 10^{-8}$	$7.61 \cdot 10^{-7}$	$4.99 \cdot 10^{-7} \dagger$	$6.40 \cdot 10^{-6} \dagger$

Table 1: All errors in conservation C_1^q for the conserved quantities and relative differences L_1^q of the primitive variables for numerical solutions of \mathcal{V}_3 . L_1^q uses the numerical solution with $\Delta x = 10/2^{11}m$ as the high resolution basis of comparison and \dagger indicates the omission of the interval $[520m, 540m]$ from the comparison.

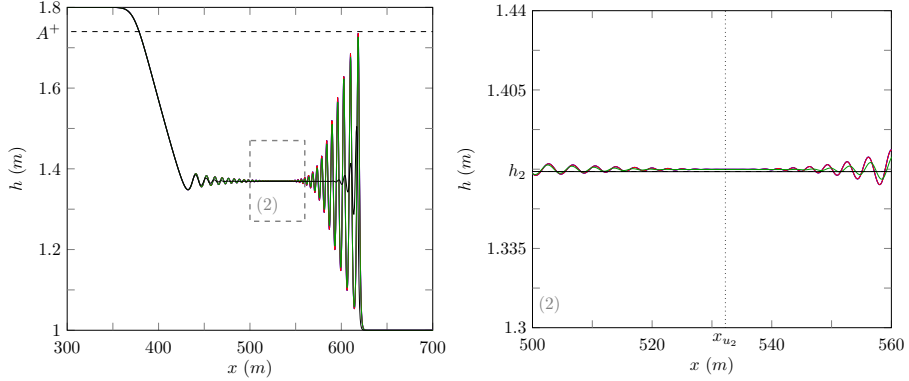


Figure 7: Numerical solutions of \mathcal{V}_3 at $t = 30s$ for the smooth dam-break problem with $\alpha = 2m$ for $\Delta x = 10/2^{10}m$ (blue), $10/2^8m$ (red), $10/2^6m$ (green) and $10/2^4m$ (black). The important quantities A^+ (dashed line), h_2 (dashed line) and x_{u2} (dotted line) are also presented.

316 require an even smaller Δx . The relative difference between numerical solutions is
 317 small and the numerical solutions exhibit good conservation. Therefore, our highest
 318 resolution numerical solution is a good approximation to any numerical solutions with
 319 lower Δx values. Figure 5 demonstrates that at $\Delta x = 10/2^{11}m$ the numerical solutions
 320 of all higher order methods are the same.

321 These results demonstrate that our highest resolution numerical solution is an accu-
 322 rate approximate solution of the Serre equations for the smoothed dam-break problem
 323 with $\alpha = 2m$. This implies that the \mathcal{S}_2 structure should be observed in solutions of the
 324 Serre equations for smooth dam-break problems with similar α values.

325 These numerical solutions compare well with those of Mitsotakis et al. [8] who
 326 use the same α but different h_0 and h_1 values and observe the \mathcal{S}_2 structure. We found
 327 that we observed this structure for all numerical method's numerical solutions to the
 328 smoothed dam-break problem with α values as low as $1m$ and $\Delta x = 10/2^{11}m$. The
 329 numerical solutions of Mitsotakis et al. [1] use $\alpha = 1m$ but different heights and observe
 330 the structure \mathcal{S}_2 . Therefore Mitsotakis et al. [1] and Mitsotakis et al. [8] observe the \mathcal{S}_2
 331 structure in their numerical results due to their choice of α for the smoothed dam-break
 332 problem.

333 The first-order method \mathcal{V}_1 is diffusive [4] and damps oscillations that are present
 334 in the numerical solutions of higher-order methods as in Figure 5. We find that for any
 335 smoothed dam-break problem with $\alpha \leq 4m$ and the dam-break problem only the \mathcal{S}_2
 336 structure is observed for the numerical solutions of \mathcal{V}_1 at $t = 30s$ with $\Delta x = 10/2^{11}m$.
 337 This is evident in Figure 8 with the numerical solutions of \mathcal{V}_1 using our finest grid
 338 where $\Delta x = 10/2^{11}m$ on our steepest initial conditions where $\alpha = 0.001m$. Therefore,
 339 Le Métayer et al. [2] using the diffusive \mathcal{V}_1 with their chosen Δx and Δt , which are
 340 larger than our Δx and Δt could only observe the \mathcal{S}_2 structure.

341 5.1.3. Node Structure

342 The “node” structure, \mathcal{S}_3 was observed by El et al. [7]. The \mathcal{S}_3 structure has os-
 343 cillations throughout regions III and IV that decay to a node at x_{u2} as can be seen in

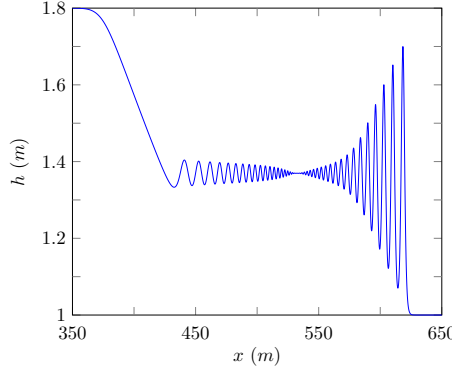


Figure 8: Numerical solution of \mathcal{V}_1 at $t = 30s$ for the smooth dam-break problem with $\alpha = 0.001m$ for $\Delta x = 10/2^{11}m$ (—).

344 Figure 9 where $\alpha = 0.4m$.

345 Figure 9 demonstrates that our numerical solutions have not converged, however
 346 this is only in the area around x_{u_2} . Due to the large difference in numerical solutions
 347 around x_{u_2} the L_1 measure over the area around x_{u_2} would not be insightful. However,
 348 by omitting this region we can gain some knowledge about how well our solutions
 349 agree away from x_{u_2} . This was performed for the relevant L_1 measures in Table 1
 350 by omitting the interval [520m, 540m]. These modified L_1 measures demonstrate that
 351 while our numerical results have visually converged outside this interval, they have not
 352 converged down to round-off error.

353 Table 1 demonstrates that the C_1 measures are still decreasing and have only at-
 354 tained round-off error for h . Therefore, to resolve the desired convergence of the nu-
 355 mercial solutions to one with small error in conservation using \mathcal{V}_3 would require even
 356 smaller Δx values.

357 There is good agreement across different numerical methods for $\Delta x = 10/2^{11}m$ as
 358 can be seen in Figure 10. In particular all the higher-order methods exhibit the same
 359 structure and only disagree in a very small region around x_{u_2} . We observe that the
 360 numerical solution of the worst higher-order method \mathcal{E} has not converged well to the
 361 numerical solutions of the other higher-order methods.

362 We have only obtained a good approximation to the desired numerical solution as
 363 $\Delta x \rightarrow 0$ away from x_{u_2} . However, our highest resolution numerical solutions from
 364 various higher-order methods are very similar. This suggests that again although we
 365 do not have full convergence, our highest resolution numerical solution is a good ap-
 366 proximation to the desired numerical solution over the whole domain. Therefore, our
 367 highest resolution numerical solutions are an accurate representation of the solutions of
 368 the Serre equations for this smoothed dam-break problem. Therefore, the \mathcal{S}_3 structure
 369 should be observed in the solutions of the Serre equations for the smoothed dam-break
 370 problem with $\alpha = 0.4m$.

371 These numerical solutions support the findings of El et al. [7] who also use some
 372 smoothing [16] but do not report what smoothing was performed. Using their method
 373 \mathcal{E} and similar Δx to El et al. [7] we observe the \mathcal{S}_4 “growth” structure in the numerical

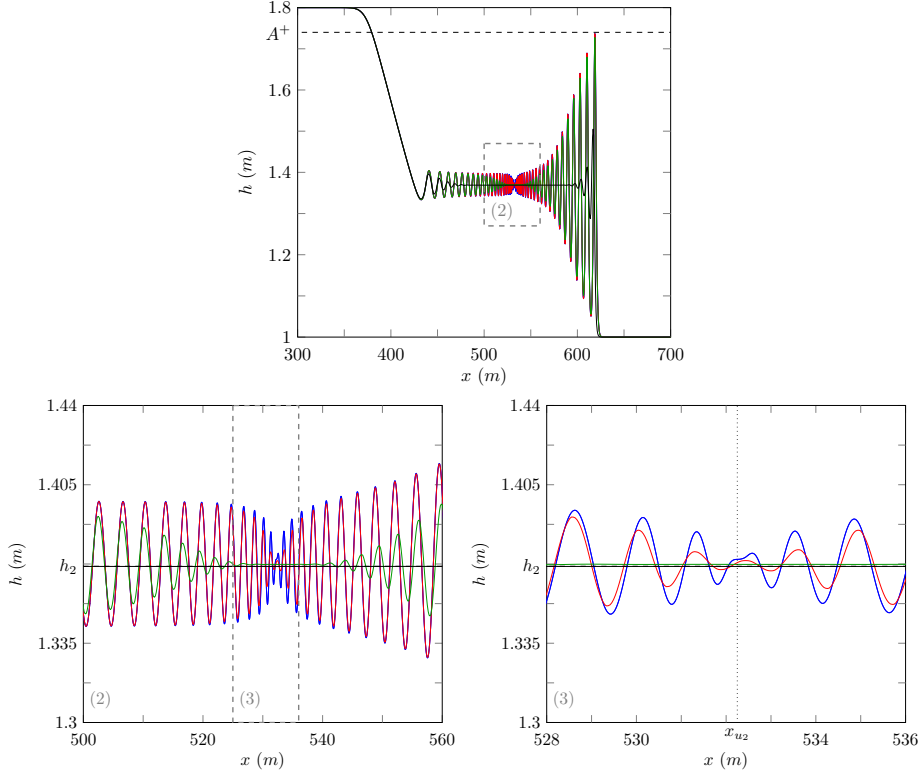


Figure 9: Numerical solutions of \mathcal{V}_3 at $t = 30s$ for the smooth dam-break problem with $\alpha = 0.4m$ for $\Delta x = 10/2^{10}m$ (blue), $10/2^8m$ (red), $10/2^6m$ (green) and $10/2^4m$ (black). The important quantities A^+ (— —), h_2 (— —) and x_{u2} (· · ·) are also presented.

374 solution for α values smaller than $0.1m$, indicating that the smoothing performed by El
375 et al. [7] limited their observed behaviour to just the \mathcal{S}_3 structure.

376 5.1.4. Growth Structure

377 The \mathcal{S}_4 “growth” structure, which has hitherto not been commonly published in
378 the literature features a growth in the oscillation amplitude around x_{u2} . An example
379 of the growth structure can be seen for \mathcal{V}_3 ’s numerical solutions in Figure 11 to the
380 smoothed dam-break problem with $\alpha = 0.1m$. This structure was observed in the
381 numerical solutions of \mathcal{V}_3 for $\Delta x = 10/2^{11}m$ at $t = 30s$ for α values as low as $0.001m$
382 and even for the dam-break problem.

383 Figure 11 shows that this structure can only be observed for $\Delta x = 10/2^{10}m$, with
384 poor convergence of the numerical results around x_{u2} . Again our L_1 measures in Table
385 1 omit the interval $[520m, 540m]$ in the numerical solutions. This demonstrates that
386 although we have visual convergence away from x_{u2} , our numerical solutions have not
387 converged to round-off error as $\Delta x \rightarrow 0$. The C_1 measures in Table 1 are still decreasing
388 and have only attained round-off error for h , although for uh and \mathcal{H} the errors in
389 conservation are small. These measures continue the trend in Table 1 where smaller α ’s

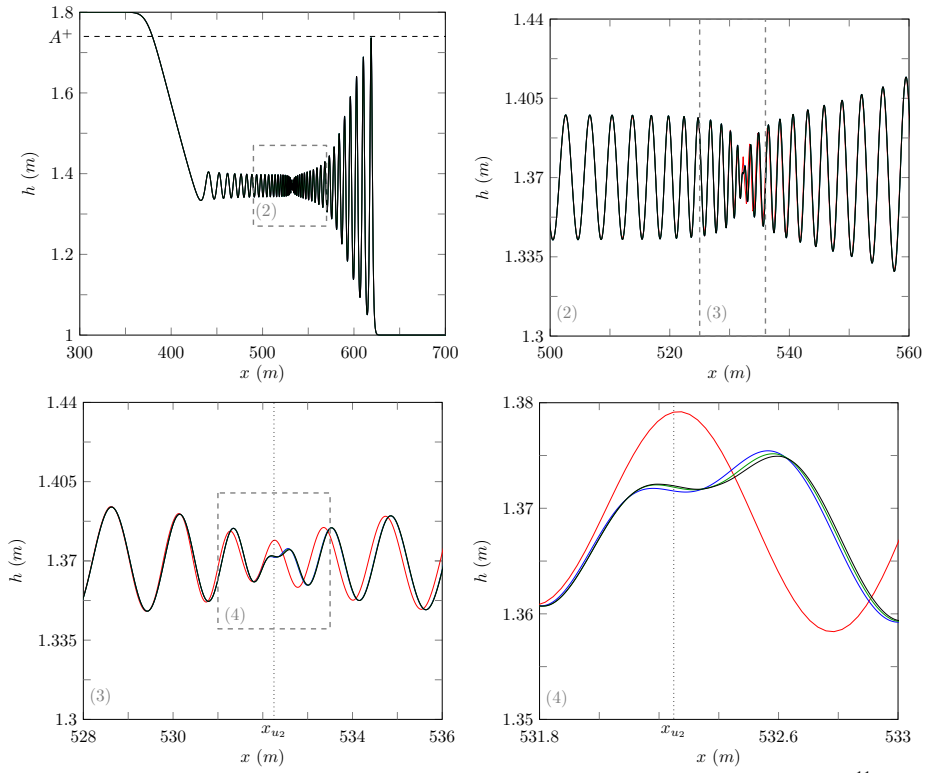


Figure 10: Numerical solutions of \mathcal{D} (blue), \mathcal{E} (red), \mathcal{V}_3 (green) and \mathcal{V}_2 (black) at $t = 30s$ with $\Delta x = 10/2^{11}m$ for the smoothed dam-break problem with $\alpha = 0.4m$. The important quantities A^+ (—) and x_{u_2} (···) are also presented.

390 and thus steeper initial conditions lead to larger L_1 and C_1 measures because steeper
391 problems are more difficult to solve accurately.

392 Figure 12 demonstrates that our numerical solutions for $\Delta x = 10/2^{11}m$ with the
393 best methods \mathcal{D} , \mathcal{V}_3 and \mathcal{V}_2 disagree for only a few oscillations around x_{u_2} . Since
394 both \mathcal{D} and \mathcal{E} are second-order finite difference methods their errors are dispersive.
395 These dispersive errors cause the numerical solutions to overestimate the oscillation
396 amplitude of the true solution, particularly around x_{u_2} . Because the dispersive errors of
397 \mathcal{E} are larger than \mathcal{D} more oscillations are observed for the numerical solutions produced
398 by \mathcal{E} . The \mathcal{V}_3 method was shown to be diffusive by Zoppou et al. [4] and therefore
399 its numerical solutions underestimate the oscillation amplitude in the true solution.
400 Therefore, the true solution of the Serre equations should be between the dispersive
401 method \mathcal{D} and the diffusive method \mathcal{V}_3 , and thus will possess the \mathcal{S}_4 structure.

402 The numerical solutions of \mathcal{D} and \mathcal{V}_3 acting as upper and lower bounds respectively
403 for the oscillation amplitude as Δx is reduced is demonstrated in Figure 13 using
404 the maximum of h in the interval [520m, 540m]. From this figure it is clear that the
405 amplitudes of the numerical solutions of \mathcal{D} converge down to the limit as the resolution
406 is increased while the numerical solution amplitudes of \mathcal{V}_3 converge up to it. This
407 shows that we have effectively bounded the true solution of the Serre equations. Un-
408 fortunately, \mathcal{V}_3 could not be run in reasonable computational times with lower Δx , but
409 the numerical solutions of \mathcal{D} show that doing so is unnecessary.

410 These results indicate that the solutions of the Serre equations to the smoothed
411 dam-break problem with sufficiently small α values should exhibit a growth structure at
412 $t = 30s$, even though we have not precisely resolved all the oscillations in our numerical
413 solutions.

414 It was found that decreasing α did increase the amplitude of the oscillations around
415 x_{u_2} . For \mathcal{V}_3 with $\Delta x = 10/2^{11}m$ and $\alpha = 0.001m$ the oscillations in h were bounded
416 by the interval [1.28m, 1.46m]. Of particular note is that the number of oscillations are
417 the same in Figures 10 and 12 for the best methods even though they have different
418 structures.

419 By changing the interval and desired time for the numerical solution, Δx could be
420 lowered further so that by $t = 3s$ our numerical solutions have fully converged for α
421 values as low as 0.001m. This allows us to show that the height of the oscillations
422 around x_{u_2} for the solution of the Serre equation to the smoothed dam-break problem
423 are bounded at $t = 3s$ as $\alpha \rightarrow 0$. Figure 14 demonstrates this for the numerical solutions
424 of \mathcal{V}_3 with $\Delta x = 10/2^{13}m$.

425 5.2. Shallow water wave equation comparison

426 The analytical solutions of the shallow water wave equations have been used as a
427 guide for the mean behaviour of the solution of the Serre equations for the dam-break
428 problem in the literature [2, 8].

429 To assess the applicability of this the mean bore depth and mean fluid velocity in
430 the interval $[x_{u_2} - 50m, x_{u_2} + 50m]$ were calculated from our numerical solution to the
431 smoothed dam-break problem with various height ratios. These means were compared
432 to their approximations from the analytical solution of the dam-break problem for the
433 shallow water wave equations h_2 and u_2 . The results of this can be seen in Figure 15

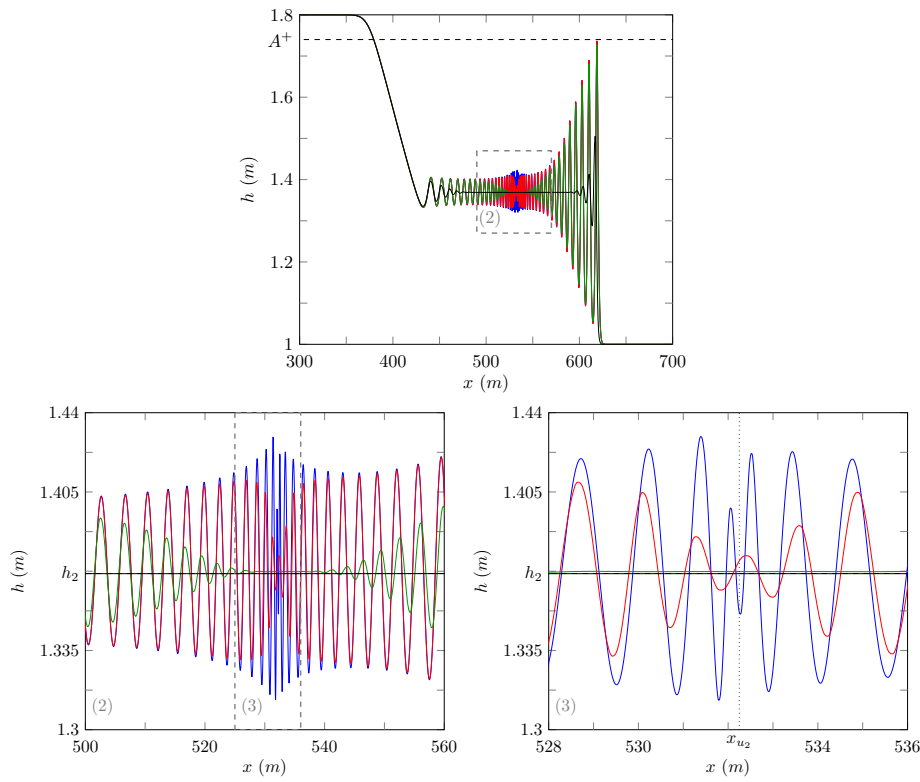


Figure 11: Numerical solutions of \mathcal{V}_3 at $t = 30s$ for the smooth dam-break problem with $\alpha = 0.1m$ for $\Delta x = 10/2^{10}m$ (blue), $10/2^8m$ (red), $10/2^6m$ (green) and $10/2^4m$ (black). The important quantities A^+ (dashed line), h_2 (dashed line) and x_{u2} (dotted line) are also presented.

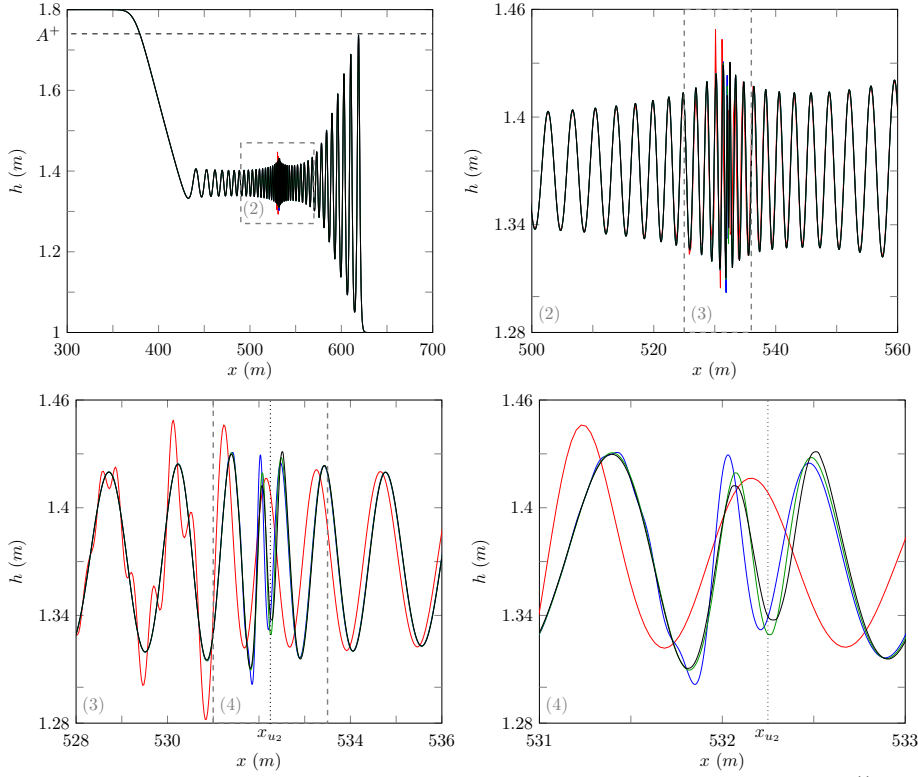


Figure 12: Numerical solutions of \mathcal{D} (blue), \mathcal{E} (red), \mathcal{V}_3 (green) and \mathcal{V}_2 (black) at $t = 30s$ with $\Delta x = 10/2^{11}m$ for the smoothed dam-break problem with $\alpha = 0.1m$. The important quantities A^+ (—) and x_{u2} (···) are also presented.

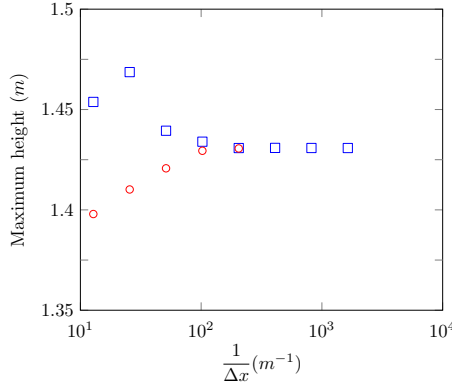


Figure 13: Maximum height of numerical solution of the smoothed dam-break problem with $\alpha = 0.4m$ at $t = 30s$ inside the interval [520m,540m] using \mathcal{D} (□) and \mathcal{V}_3 (○).

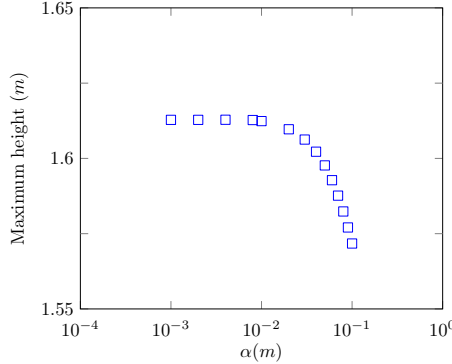


Figure 14: Maximum height of numerical solution around x_{u_2} at $t = 3s$ of various smoothed dam-break problem as α decreases, using \mathcal{V}_3 (□) with $\Delta x = 10/2^{13}m$.

434 for numerical solutions of \mathcal{V}_3 with $\Delta x = 10/2^9m$ to the smoothed dam-break problem
 435 at $t = 100s$ with $\alpha = 0.1m$ where h_0 is fixed and h_1 is varied.

436 We use a final time of $t = 100s$ as it allows the internal structure of the bore to
 437 develop more fully giving a more reliable mean estimate, as a consequence we resort
 438 to a coarser grid to keep the run-times reasonable. We find that decreasing Δx does
 439 not significantly alter the mean of h and u . We also find that increasing α also does
 440 not significantly alter the mean of h and u . Therefore, the mean behaviour of the true
 441 solution of the Serre equations to the dam-break problem is captured by these numerical
 442 solutions, if it exists.

443 It can be seen that h_2 and u_2 are good approximations to the mean behaviour of
 444 the fluid inside the bore for a range of different aspect ratios. Although, as h_1/h_0
 445 increases this approximation becomes worse, so that h_2 becomes an underestimate and
 446 consequently u_2 is an overestimate.

447 We find that for $h_1/h_0 = 1.8$ the mean values of h and u inside the bore for the Serre
 448 equations are not equal to h_2 and u_2 . This can be seen in Figure 16 for the numerical
 449 solutions of \mathcal{V}_3 with $\Delta x = 10/2^9m$ to the smoothed dam-break problem with $\alpha = 0.1m$
 450 at $t = 300s$. It can be seen that h_2 is an underestimate of h and u_2 is an overestimate
 451 of u although the difference between these values and the mean behaviour of the Serre
 452 equations is small and only noticeable over long time periods.

453 The location of the leading wave of the Serre equations slowly diverges from the
 454 location of the front of a bore in the shallow water wave equations over long periods of
 455 time. This divergence causes the small difference evident in \mathcal{V}_3 's numerical solution
 456 to the smoothed dam-break problem with $\alpha = 0.1m$ at $t = 300s$ using $\Delta x = 10/2^9m$,
 457 which is shown in Figure 17.

458 We note that the S_4 structure present in the numerical solutions using this method
 459 and parameters at $t = 30s$ in Figure 11 has decayed away by $t = 300s$ in Figure
 460 16. This is a trend throughout our numerical solutions where oscillation amplitude
 461 decreases over time around x_{u_2} , changing the structure of the solution. This can be seen
 462 by obtaining full convergence of the numerical solutions to the smoothed dam-break
 463 problem at $t = 3s$. The converged to numerical solutions for \mathcal{V}_3 are shown in Figure
 464 18. From this figure it can be seen that the oscillation amplitudes for the numerical

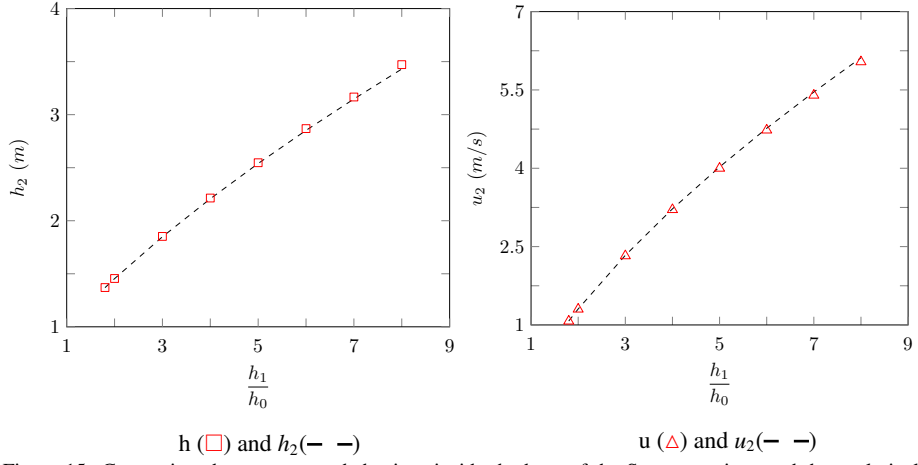


Figure 15: Comparison between mean behaviour inside the bore of the Serre equations and the analytical solution of the shallow water wave equations for a range of different aspect ratios.

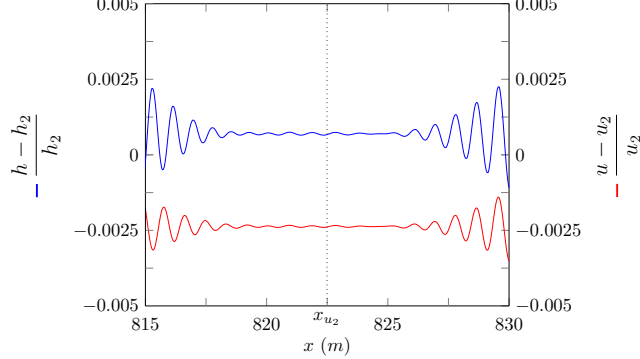


Figure 16: The relative difference between h and u and their comparisons h_2 and u_2 plotted around x_{u_2} (---) for \mathcal{V}_3 's solutions with $\Delta x = 10/2^9 m$ for the smoothed dam-break problem with $\alpha = 0.1m$ at $t = 300s$.

solutions for the smoothed dam-break problems with $\alpha = 0.4m$ and $\alpha = 0.1m$ are much larger at $t = 3s$ than they are at $t = 30s$ in Figure 4. Since we have demonstrated that our numerical solutions are good approximations to the true solution of the Serre equations at $t = 30s$ and $t = 3s$, decreasing oscillation amplitude around x_{u_2} over time is probably a property of the Serre equations. This implies that bounding the oscillation amplitudes at time $t = 3s$ as was done above, bounds the oscillation amplitudes at all later times.

5.2.1. Contact discontinuity

El et al. [7] noted the presence of a ‘degenerate contact discontinuity’ which is the node in the S_3 structure and travels at the mean fluid velocity in the bore.

We observe that as our numerical solutions evolve over time, oscillations appear to be released from the contact discontinuity and travel away from it in both directions, leading to decay of amplitudes around the contact discontinuity. Therefore, the contact

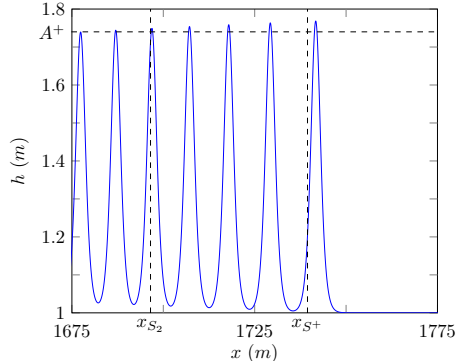


Figure 17: Numerical solution of \mathcal{V}_3 with $\Delta x = 10/2^9 m$ for the smoothed dam-break problem with $\alpha = 0.1 m$ at $t = 300 s$ around the front of the undular bore. The important quantities A^+ (— —), x_{S_2} (— —) and x_{S^+} (— —) are also presented.

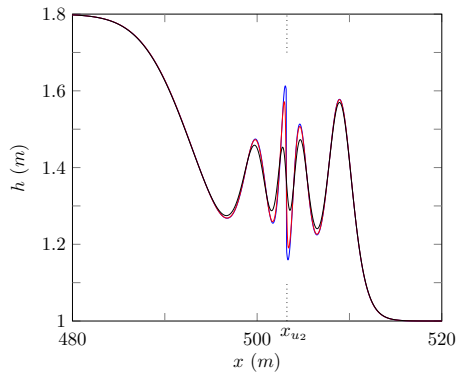


Figure 18: Numerical solution of \mathcal{V}_3 with $\Delta x = 10/2^{13} m$ for the smoothed dam-break problem with $\alpha = 0.001 m$ (blue), $0.1 m$ (red) and $0.4 m$ (black) at $t = 3 s$. For comparison x_{u2} (· · ·) is also plotted.

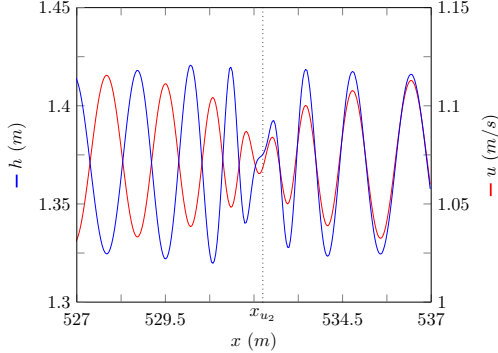


Figure 19: Numerical solution of \mathcal{V}_3 's with $\Delta x = 10/2^9 m$ for the smoothed dam-break problem with $\alpha = 0.1m$ at $t = 30s$ around the contact discontinuity close to x_{u_2} (· · ·).

discontinuity is an important feature and its behaviour determines the structure of the oscillations in the middle of the undular bore.

The different speeds of the oscillations are determined by the phase velocity, which for the Serre equations linearised around the mean height \bar{h} and mean velocity \bar{u} in regions III and IV of the solution to the dam-break problem is

$$v_p = \bar{u} \pm \sqrt{g\bar{h}} \sqrt{\frac{3}{\bar{h}^2 k^2 + 3}} \quad (10)$$

with wave number k . It can be seen that as $k \rightarrow \infty$ then $v_p \rightarrow \bar{u}$ and as $k \rightarrow 0$ then $v_p \rightarrow \bar{u} \pm \sqrt{g\bar{h}}$. Since the contact discontinuity travels at the mean velocity inside the bore, it corresponds to very high wave number oscillations. The oscillations on the left travel slower than the contact discontinuity and are therefore lower wave number oscillations associated with the phase velocity $\bar{u} - \sqrt{g\bar{h}} \sqrt{3/(\bar{h}^2 k^2 + 3)}$. The oscillations on the right travel quicker than the contact discontinuity and are therefore lower wave number oscillations associated with the phase velocity $\bar{u} + \sqrt{g\bar{h}} \sqrt{3/(\bar{h}^2 k^2 + 3)}$.

These different phase velocities have two different behaviours for h and u . When the phase velocity is $\bar{u} + \sqrt{g\bar{h}} \sqrt{3/(\bar{h}^2 k^2 + 3)}$ we have oscillations where h and u are in-phase, while when the phase velocity is $\bar{u} - \sqrt{g\bar{h}} \sqrt{3/(\bar{h}^2 k^2 + 3)}$ we have oscillations where h and u are out-of-phase. This can be seen in Figure 19 for the numerical solutions of \mathcal{V}_3 with $\Delta x = 10/2^9 m$ for the smoothed dam-break problem with $\alpha = 0.1m$ at $t = 30s$.

5.3. Whitham Modulation Comparsion

El et al. [7] demonstrated that their Whitham modulation results approximated the numerical solutions of the smoothed dam-break problem well for a range of aspect ratios. We observed that the Whitham modulation results are an underestimate compared to our numerical solutions.

This can be seen in Figure 20 as the relative difference between A^+ from El et al. [7] and the leading wave amplitude of our numerical solution A does not converge to 0 over time. Since we find that the numerical solutions for the smoothed dam-break problem

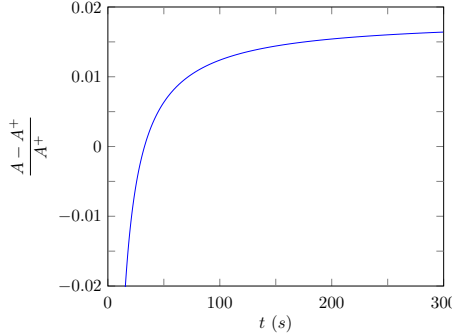


Figure 20: Relative difference between Whitham modulation result A^+ and the leading wave amplitude A from our numerical solutions of \mathcal{V}_3 with $\Delta x = 10/2^9 m$ for the smoothed dam-break problem with $\alpha = 0.1m$ over time.

506 with $\alpha = 0.1m$ have converged for the front of the undular bore by $\Delta x = 10/2^8 m$ as
507 in Figure 11, our numerical solutions for A are considered reliable. We also note that
508 unlike the oscillations around x_{u_2} , the leading wave amplitude increases over time.

509 The Whitham modulation results for the location of the leading wave x_{S^+} is a better
510 approximation than that given by the shallow water wave equations x_{S_2} , as can be seen
511 in Figure 17.

512 6. Conclusions

513 Utilising two finite difference methods of second-order and three finite difference
514 finite volume methods of various orders to solve the nonlinear weakly dispersive Serre
515 equations an investigation into the smoothed dam-break problem with varying steep-
516 ness was performed. Four different structures of the numerical solutions were observed
517 and demonstrated to be valid, the general trend of these structures is that an increase
518 in steepness increases the size and number of oscillations in the solution. This study
519 explains the different structures exhibited by the numerical results in the literature for
520 the smoothed dam-break problem for the Serre equations and uncovers a new result.
521 These results demonstrate that other methods in the literature could replicate our results
522 if their simulations are extended. Furthermore, these results suggest that this new result
523 and its associated structure is to be expected for the solution of the Serre equation to
524 the dam-break problem at least for short enough time spans, if it exists.

525 We find that the analytical solution of the shallow water wave equations for the
526 dam-break problem provides a reasonable approximation to the mean height and veloc-
527 ity inside the bore formed by the smoothed dam-break problem for the Serre equations.
528 Finally, we observe that the Whitham modulations results for the leading wave of an
529 undular bore provide a more accurate approximation to the location and depth of the
530 front of an undular bore than the shallow water wave equations.

- 531 [1] D. Mitsotakis, D. Dutykh, J. Carter, On the nonlinear dynamics of the traveling-
532 wave solutions of the Serre system, Wave Motion 70 (1) (2017) 166–182.

- 533 [2] O. Le Métayer, S. Gavrilyuk, S. Hank, A numerical scheme for the Green-Naghdi
 534 model, *Journal of Computational Physics* 229 (6) (2010) 2034–2045.
- 535 [3] C. Zoppou, S. Roberts, J. Pitt, A Solution of the Conservation Law Form of the
 536 Serre Equations, *The ANZIAM Journal* 57 (4) (2017) 385–394.
- 537 [4] C. Zoppou, J. Pitt, S. Roberts, Numerical Solution of the Fully Non-Linear
 538 Weakly Dispersive Serre Equations for Steep Gradient Flows, *Applied Mathematical Modelling* 48 (2017) 70–95.
- 540 [5] P. Bonneton, E. Barthélemy, F. Chazel, R. Cienfuegos, D. Lannes, F. Marche,
 541 M. Tissier, Recent advances in Serre-Green Naghdi modelling for wave transfor-
 542 mation, breaking and runup processes, *European Journal of Mechanics B/Fluids*
 543 30 (6) (2011) 589–597.
- 544 [6] P. Bonneton, F. Chazel, D. Lannes, F. Marche, M. Tissier, A splitting approach
 545 for the fully nonlinear and weakly dispersive Green-Naghdi model, *Journal of*
 546 *Computational Physics* 230 (4) (2011) 1479–1498.
- 547 [7] G. El, R. H. J. Grimshaw, N. F. Smyth, Unsteady undular bores in fully nonlinear
 548 shallow-water theory, *Physics of Fluids* 18 (2) (2006) 027104.
- 549 [8] D. Mitsotakis, B. Ilan, D. Dutykh, On the Galerkin/Finite-Element Method for
 550 the Serre Equations, *Journal of Scientific Computing* 61 (1) (2014) 166–195.
- 551 [9] C. H. Su, C. S. Gardner, Korteweg-de Vries equation and generalisations. III.
 552 Derivation of the Korteweg-de Vries equation and Burgers equation, *Journal of*
 553 *Mathematical Physics* 10 (3) (1969) 536–539.
- 554 [10] D. Lannes, P. Bonneton, Derivation of asymptotic two-dimensional time-
 555 dependent equations for surface water wave propagation, *Physics of Fluids* 21 (1)
 556 (2009) 16601–16610.
- 557 [11] M. Li, P. Guyenne, F. Li, L. Xu, High order well-balanced CDG-FE methods
 558 for shallow water waves by a Green-Naghdi model, *Journal of Computational*
 559 *Physics* 257 (2014) 169–192.
- 560 [12] Y. A. Li, Hamiltonian Structure and Linear Stability of Solitary Waves of the
 561 Green-Naghdi Equations, *Journal of Nonlinear Mathematical Physics* 9 (2002)
 562 99–105.
- 563 [13] A. E. Green, P. M. Naghdi, A derivation of equations for wave propagation in
 564 water of variable depth, *Journal of Fluid Mechanics* 78 (2) (1976) 237–246.
- 565 [14] C. Wu, G. Huang, Y. Zheng, Theoretical solution of dam-break shock wave, *Jour-
 566 nal of Hydraulic Engineering* 125 (11) (1999) 1210–1215.
- 567 [15] A. A. Harten, High resolution schemes for hyperbolic conservation laws, *Journal*
 568 *of Computational Physics* 49 (3) (1983) 357–393.
- 569 [16] G. El, M. Hoefer, Dispersive shock waves and modulation theory, *Physica D:*
 570 *Nonlinear Phenomena* 333 (2016) 11–65.

571 **Appendix A.**

572 The methods \mathcal{E} and \mathcal{D} use the centred second-order finite difference approximation
 573 to the momentum equation (1b), denoted as \mathcal{D}_u . For the mass equation (1a) \mathcal{E} uses the
 574 two step Lax-Wendroff method, denoted as \mathcal{E}_h while \mathcal{D} uses a centred second-order
 575 finite difference approximation, denoted as \mathcal{D}_h .

576 *Appendix A.1. \mathcal{D}_u for the Momentum Equation*

577 First (1b) is expanded to get

$$578 \quad h \frac{\partial u}{\partial t} - h^2 \frac{\partial^2 u}{\partial x \partial t} - \frac{h^3}{3} \frac{\partial^3 u}{\partial x^2 \partial t} = -X$$

580 where X contains only spatial derivatives and is

$$581 \quad X = uh \frac{\partial u}{\partial x} + gh \frac{\partial h}{\partial x} + h^2 \frac{\partial u}{\partial x} \frac{\partial u}{\partial x} + \frac{h^3}{3} \frac{\partial u}{\partial x} \frac{\partial^2 u}{\partial x^2} - h^2 u \frac{\partial^2 u}{\partial x^2} - \frac{h^3}{3} u \frac{\partial^3 u}{\partial x^3}.$$

583 All derivatives are approximated by second-order centred finite difference approximations
 584 on a uniform grid in space and time, which after rearranging into an update
 585 formula becomes

$$586 \quad h_i^n u_i^{n+1} - (h_i^n)^2 \left(\frac{u_{i+1}^{n+1} - u_{i-1}^{n+1}}{2\Delta x} \right) - \frac{(h_i^n)^3}{3} \left(\frac{u_{i+1}^{n+1} - 2u_i^{n+1} + u_{i-1}^{n+1}}{\Delta x^2} \right) = -Y_i^n \quad (\text{A.1})$$

588 where

$$589 \quad Y_i^n = 2\Delta t X_i^n - h_i^n u_i^{n-1} + (h_i^n)^2 \left(\frac{u_{i+1}^{n-1} - u_{i-1}^{n-1}}{2\Delta x} \right) + \frac{(h_i^n)^3}{3} \left(\frac{u_{i+1}^{n-1} - 2u_i^{n-1} + u_{i-1}^{n-1}}{\Delta x^2} \right)$$

591 and

$$593 \quad X_i^n = u_i^n h_i^n \frac{u_{i+1}^n - u_{i-1}^n}{2\Delta x} + gh_i^n \frac{h_{i+1}^n - h_{i-1}^n}{2\Delta x} + (h_i^n)^2 \left(\frac{u_{i+1}^n - u_{i-1}^n}{2\Delta x} \right)^2 \\ 594 \quad + \frac{(h_i^n)^3}{3} \frac{u_{i+1}^n - u_{i-1}^n}{2\Delta x} \frac{u_{i+1}^n - 2u_i^n + u_{i-1}^n}{\Delta x^2} - (h_i^n)^2 u_i^n \frac{u_{i+1}^n - 2u_i^n + u_{i-1}^n}{\Delta x^2} \\ 595 \quad - \frac{(h_i^n)^3}{3} u_i^n \frac{u_{i+2}^n - 2u_{i+1}^n + 2u_{i-1}^n - u_{i-2}^n}{2\Delta x^3}.$$

597 Equation (A.1) can be rearranged into an explicit update scheme \mathcal{D}_u for u given its
 598 current and previous values, so that

$$599 \quad \begin{bmatrix} u_0^{n+1} \\ \vdots \\ u_m^{n+1} \end{bmatrix} = A^{-1} \begin{bmatrix} -Y_0^n \\ \vdots \\ -Y_m^n \end{bmatrix} =: \mathcal{D}_u(\mathbf{u}^n, \mathbf{h}^n, \mathbf{u}^{n-1}, \Delta x, \Delta t) \quad (\text{A.2})$$

601 where A is a tri-diagonal matrix.

602 *Appendix A.2. Numerical Methods for the Mass Equation*

603 The two step Lax-Wendroff update \mathcal{E}_h for h is

$$604 \quad h_{i+1/2}^{n+1/2} = \frac{1}{2} (h_{i+1}^n + h_i^n) - \frac{\Delta t}{2\Delta x} (u_{i+1}^n h_{i+1}^n - h_i^n u_i^n), \\ 605 \\ 606$$

$$607 \quad h_{i-1/2}^{n+1/2} = \frac{1}{2} (h_i^n + h_{i-1}^n) - \frac{\Delta t}{2\Delta x} (u_i^n h_i^n - h_{i-1}^n u_{i-1}^n) \\ 608$$

609 and

$$610 \quad h_i^{n+1} = h_i^n - \frac{\Delta t}{\Delta x} (u_{i+1/2}^{n+1/2} h_{i+1/2}^{n+1/2} - u_{i-1/2}^{n+1/2} h_{i-1/2}^{n+1/2}). \\ 611 \\ 612$$

612 The quantities $u_{i\pm 1/2}^{n+1/2}$ are calculated using u^{n+1} obtained by applying \mathcal{D}_u (A.2) to u^n
613 then linearly interpolating in space and time to give

$$614 \quad u_{i+1/2}^{n+1/2} = \frac{u_{i+1}^{n+1} + u_{i+1}^n + u_i^{n+1} + u_i^n}{4} \\ 615$$

616 and

$$617 \quad u_{i-1/2}^{n+1/2} = \frac{u_i^{n+1} + u_i^n + u_{i-1}^{n+1} + u_{i-1}^n}{4}. \\ 618$$

619 Thus we have the following update scheme \mathcal{E}_h for (1a)

$$620 \quad \mathbf{h}^{n+1} = \mathcal{E}_h(\mathbf{u}^n, \mathbf{h}^n, \mathbf{u}^{n+1}, \Delta x, \Delta t). \quad (\text{A.3}) \\ 621$$

622 The second order centered finite difference approximation to the conservation of
623 mass equation (1a) is

$$624 \quad h_i^{n+1} = h_i^{n-1} - \Delta t \left(u_i^n \frac{h_{i+1}^n - h_{i-1}^n}{\Delta x} + h_i^n \frac{u_{i+1}^n - u_{i-1}^n}{\Delta x} \right). \\ 625$$

626 Thus we have an update scheme \mathcal{D}_h for all i

$$627 \quad \mathbf{h}^{n+1} = \mathcal{D}_h(\mathbf{u}^n, \mathbf{h}^n, \mathbf{h}^{n-1}, \Delta x, \Delta t). \quad (\text{A.4}) \\ 628$$

629 *Appendix A.3. Complete Method*

630 The method \mathcal{E} is the combination of (A.3) for (1a) and (A.2) for (1b) in the follow-
631 ing way

$$632 \quad \begin{aligned} \mathbf{u}^{n+1} &= \mathcal{D}_u(\mathbf{u}^n, \mathbf{h}^n, \mathbf{u}^{n-1}, \Delta x, \Delta t) \\ \mathbf{h}^{n+1} &= \mathcal{E}_h(\mathbf{u}^n, \mathbf{h}^n, \mathbf{u}^{n+1}, \Delta x, \Delta t) \end{aligned} \quad \left\{ \mathcal{E}(\mathbf{u}^n, \mathbf{h}^n, \mathbf{u}^{n-1}, \mathbf{h}^{n-1}, \Delta x, \Delta t) \right\}. \quad (\text{A.5}) \\ 633$$

634 The method \mathcal{D} is the combination of (A.4) for (1a) and (A.2) for (1b) in the follow-
635 ing way

$$636 \quad \begin{aligned} \mathbf{h}^{n+1} &= \mathcal{D}_h(\mathbf{u}^n, \mathbf{h}^n, \mathbf{h}^{n-1}, \Delta x, \Delta t) \\ \mathbf{u}^{n+1} &= \mathcal{D}_u(\mathbf{u}^n, \mathbf{h}^n, \mathbf{u}^{n-1}, \Delta x, \Delta t) \end{aligned} \quad \left\{ \mathcal{D}(\mathbf{u}^n, \mathbf{h}^n, \mathbf{u}^{n-1}, \mathbf{h}^{n-1}, \Delta x, \Delta t) \right\}. \quad (\text{A.6}) \\ 637$$